HHS Public Access

Author manuscript

Biomed Microdevices. Author manuscript; available in PMC 2015 June 22.

Published in final edited form as:

Biomed Microdevices. 2008 August ; 10(4): 585–595. doi:10.1007/s10544-008-9170-y.

Synthetic microvascular networks for quantitative analysis of particle adhesion

Balabhaskar Prabhakarpandian,
Biomedical Technology, CFD Research Corporation, 215 Wynn Dr., Huntsville, AL 35805, USA

Kapil Pant,
Biomedical Technology, CFD Research Corporation, 215 Wynn Dr., Huntsville, AL 35805, USA

Robert C. Scott,
Department of Mechanical Engineering, Temple University, 1947 North 12th Street, Philadelphia, PA 19122, USA

Christopher B. Patillo,
Department of Mechanical Engineering, Temple University, 1947 North 12th Street, Philadelphia, PA 19122, USA

Daniel Irimia,
BioMEMS Resource Center, Massachusetts General Hospital, 114 16th Street, Room 1239, Charlestown, MA 02129-4404, USA

Mohammad F. Kiani, and
Department of Mechanical Engineering, Temple University, 1947 North 12th Street, Philadelphia, PA 19122, USA

Department of Radiation Oncology, Temple University, 1947 North 12th Street, Philadelphia, PA 19122, USA

Shivshankar Sundaram
Biomedical Technology, CFD Research Corporation, 215 Wynn Dr., Huntsville, AL 35805, USA

Abstract

We have developed a methodology to study particle adhesion in the microvascular environment using microfluidic, image-derived microvascular networks on a chip accompanied by Computational Fluid Dynamics (CFD) analysis of fluid flow and particle adhesion. Microfluidic networks, obtained from digitization of *in vivo* microvascular topology were prototyped using soft-lithography techniques to obtain semicircular cross sectional microvascular networks in polydimethylsiloxane (PDMS). Dye perfusion studies indicated the presence of well-perfused as well as stagnant regions in a given network. Furthermore, microparticle adhesion to antibody coated networks was found to be spatially non-uniform as well. These findings were broadly corroborated in the CFD analyses. Detailed information on shear rates and particle fluxes in the entire network, obtained from the CFD models, were used to show global adhesion trends to be

sxs@cfdrc.com.

qualitatively consistent with current knowledge obtained using flow chambers. However, in comparison with a flow chamber, this method represents and incorporates elements of size and complex morphology of the microvasculature. Particle adhesion was found to be significantly localized near the bifurcations in comparison with the straight sections over the entire network, an effect not observable with flow chambers. In addition, the microvascular network chips are resource effective by providing data on particle adhesion over physiologically relevant shear range from even a single experiment. The microfluidic microvascular networks developed in this study can be readily used to gain fundamental insights into the processes leading to particle adhesion in the microvasculature.

Keywords

Microvascular; Network; Particle; Microcirculation; Microfluidics; CFD; Shear; Adhesion; Delivery

1 Introduction

It has been known for several decades that during many pathological conditions the vascular surface of the endothelium is altered (Rao et al. 2007; Molla and Panes 2007; Kluger 2004; Pasyk and Jakobczak 2004; Prabhakarpandian et al. 2001; Muller and Griesmacher 2000; Nguyen et al. 2000; Cotran and Mayadas-Norton 1998; Springer 1994). A key paradigm in this alteration is that certain endothelial cell adhesion molecules are inducible. That is, they are expressed at a low level, if at all, on endothelium within normal tissue, but dramatically upregulated in response to appropriate biochemical stimuli (Carlos and Harlan 1994).

Concomitantly, with the recent advent of novel particle design and formulation methods there has been a veritable explosion in the number of particulate systems that have been engineered for targeted drug delivery in various therapeutic applications (see review by Moghimi et al. 2005). Delivery vehicles under development include polymeric micelles and nanoparticles, liposomes, polyplexes, dendrimers, viral-derived capsid nanoparticles. These platforms offer great flexibility with the ability of therapeutic and/or diagnostic agents to be encapsulated in, covalently attached to, or adsorbed on to these drug carriers. However, along with this diversity and flexibility comes the issue of choice. Careful selection and optimization of these drug particle properties is needed to attain the promise of maximal efficacy while simultaneously minimizing side effects.

In combination, the recognition of these drastically different endothelial surfaces and the development of novel particulates have led to the concept of endothelial cell adhesion molecule mediated targeted drug delivery (Scott et al. 2007; Hajitou et al. 2006; Patillo et al. 2005; Bendas et al. 1999; Spragg et al. 2003; Bloemen et al. 1995). However, in many cases these targeting schemes are not successful, in part, because the mechanics of particle (cell or drug carrier) adhesion to tissue (vascular endothelium) is not sufficiently understood. The probability of adhesion of a particle to its target *in-vivo* depends upon the interplay of at least three major elements (a) the geometric features of the vasculature at the treatment site and the associated local hemodynamic factors such as wall shear stress, and fluidic pressure

(b) particle physicochemical properties such as size, shape and density, and (c) ligand–receptor biochemical interactions at the target site.

In the current development paradigm, *in vitro* flow chambers with idealized geometries are employed to experimentally model particle adhesion in a fluidic environment and address questions on the nature of the relationship between fluid flow (stress), particle motion (transport), ligand density or endothelial cell response, and particle attachment. These flow chambers typically consist of a transparent apparatus perfused at low Reynolds numbers to match shear conditions observed in microcirculation *in vivo*. The vessel wall is modeled by either coating with appropriate proteins or growth of cells on the lower plate of the flow chamber (Luscinskas et al. 1994). Since the advent of flow chambers, they have rapidly emerged as the mainstay for investigation of microvascular interactions in post-capillary venules (leukocyte–endothelial cell interaction, for example). These flow chambers have been used by a number of investigators, for example, to identify the roles of adhesion molecules such as E-selectin, P-selectin, and PSGL-1, and their ligands in the leukocyte adhesion cascade (Burch et al. 2002; Crutchfield et al. 2000; Patel 1999; Goetz et al. 1994; Cozens-Roberts et al. 1990).

More recently, *in vitro* flow chambers have been used to study particulate drug carrier delivery to the endothelium via upregulation of adhesion molecules (Zou et al. 2005; Sakhalkar et al. 2003; Blackwell et al. 2001; Dickerson et al. 2001; El-Sayed et al. 2001; Kiani et al. 2002). A study using an idealized *in vitro* flow chamber (Patil et al. 2001) investigated the adherence of 5-, 10-, 15-, and 20-μm diameter polystyrene microspheres with a PSGL-1 construct (Goetz et al. 1997) to P-selectin. They found that adhesion was dependent on both particle size as well as shear rate. Critical shear values, obtained from their data, matched the idealized mathematical representation codified in the Cozens-Roberts relationship (Cozens-Roberts et al. 1990).

Different types of flow chambers (e.g., parallel-plate, radial, capillary) are currently in use. However, all these flow chambers feature a common theme of idealized geometries. These simplifications have the benefit of readily characterized shear stress and other fluidic parameters, which can be used directly in the interpretation of experimental results. However, these *in vitro* flow chambers have several important limitations in modeling the *in vivo* environment. Firstly, strong evidence suggests that significant differences exist between endothelial cell function in *microvasculature* as compared with large vessels (Gerritsen 1987). In particular, post-capillary venules are the morphologically dominant region where adhesion mediated delivery takes place (Springer 1994) and hence are a focus of this study. In contrast, *in vitro* flow chambers are mostly designed to mimic larger vessel flow (shear) rates. For example, the Glycotech flow chamber (Glycotech, Gaithersburg, MD) is about 2,500 μm wide and 125 μm deep in its smallest configuration, which is significantly larger than the post capillary venules (30–70 μm in diameter). Secondly, currently available flow chambers do not realistically model the complex geometrical features found *in vivo* in the microcirculation (e.g., bifurcations, convolutions, cross-sectional area changes, tortuous path lengths). These complex features directly affect local fluid and particle dynamics (e.g., shear stress, pressure, residence time), and thereby influence the adhesion process. They also strongly impact the transport of cells and drug carriers to the targeted site. In diseased tissue

such as the ones affected by tumor growth, stenoses, arteriosclerosis, or radiation therapy, the microvasculature is strikingly different morphologically and flow profiles may exhibit abnormalities such as recirculation zones (Goldsmith and Turitto 1986). Thirdly, the interconnectedness of the microvasculature is vital to its function, allowing blood cells to migrate throughout the tissue. Studying *complete microvascular networks* provides information that cannot be obtained from analyzing randomly selected individual vessels (Gaehtgens 1992). Finally, the present flow chambers require significant amounts of reagents and cells (for example leukocytes, antibodies) and are not cost-effective (Brown and Larson 2001). They are also not disposable and require extensive cleaning/rinsing prior to reuse to minimize undesirable effects due to contamination.

Several studies have reported on the use of improved *in vitro* microvascular channels. Cokelet et al. 1993, fabricated an *in vitro* microvascular channel to study blood flow by photolithography on microscope slide glass. Another group (Frame and Sarelius 1995) generated idealized (straight) semi-circular microvascular channels (20–50 μm) on glass to mimic the arteriolar microcirculation. They were also successful in growing endothelial cells on these channels. However, both studied idealized (straight) microchannels that did not account for either the interconnectedness or variations found in *in vivo* microvascular networks.

Recently, there have been a number of studies focusing on *in vitro* culture and analysis of cellular behavior using microfluidics based devices (see reviews by El-Ali et al. 2006 and Nahmias et al. 2007). In a more closely related study focusing on adhesion (Lu et al. 2004) developed a microfluidics based variable shear device for cellular studies. However, this device used channels with widths on the range of several hundred microns and idealized constructions with uniform branching angles and linear topology, not typical of microcirculation. Furthermore, this study was focused on cell detachment forces as related to local fluid dynamics and did not address particle adhesion under dynamic flow.

Keeping in mind the limitations of currently available *in vitro* flow chambers, and enabled by recent advances in microfabrication technologies, we describe here an anatomically realistic, microfluidic device to study particle adhesion in the microvascular environment. Critical features of *in-vivo* microcirculation emulated in this model include correct size (and with physiologically appropriate perfusion rates, shear), branched and networked topology along with the ability to model cell/particle and vessel wall interactions. Microfluidic networks, obtained from digitization of *in vivo* microvascular topology, are prototyped using photo- and soft-lithography techniques (Anderson et al. 2000) to obtain semicircular cross sectional microvascular networks (hereafter referred to as the Synthetic Microvascular Networks or SMNs). Computational Fluid Dynamics (CFD) analyses of fluid flow and particle transport in the SMNs are used to provide detailed information on shear rates and particle fluxes in the entire network. Experimental results obtained from the SMNs are compared with a typical parallel plate flow chamber experiment to estimate the reagent volume savings.

2 Materials and methods

2.1 Digitization of microvascular networks

Microvascular networks were obtained from a database of images of cremaster muscle of hamsters (Syrian Golden) collected according the ANET system developed previously (Roth and Kiani 1999; Roth et al. 1999 and Nguyen et al. 2000). The images were traced and digitized using the software package Arc-Info (ESRI) into AutoCAD-MAP format. The "arc-node topology" feature in Arc-Info was used to digitize the cremaster microvascular network (Fig. 1(a)) to map the vessels. The image was then vectorized to obtain a digitized reproduction of the image (Fig. 1(b)) with the associated files, which contain the connectivity information of the network. The information on the vectorized image is in geographic information systems (GIS) format and was directly incorporated into the ANET system. Flow directions in these networks as observed *in vivo* served as guidelines for defining inlet and outlet ports in the digitized network. The digitized images of the cremaster muscle yielded networks with average size of 10 μm.

As our ultimate objective is to study adhesion in the human post-capillary venules (30–70 μm) and in view of the challenges associated with access to complete post-capillary venule *in vivo* networks, the vessel diameters were scaled using the following procedure. First, the entire network area was linearly scaled by a factor of 10 to eliminate self-intersecting vessels. Then, the individual vessels were created by scaling the *in-vivo* diameters by a factor of 3 to 6 to yield diameters ranging from 30 to 60 μm, which are more representative of the human post-capillary venules.

2.2 Microfabrication of synthetic microvascular networks

Most microfabrication processes are limited to creating channels with uniform depth (rectangular or trapezoidal cross-section). Methods to create semi-circular cross-sectioned masters are known (Daly et al. 1990). In keeping with *in-vivo* morphology, it was desired to produce channels with circular cross-section. While, in principle this can be achieved by aligning and bonding two PDMS layers, doing so within the desired tolerance (1–2 μm) over a wide network area was beyond the scope of this effort. Hence we decided to adopt semi-circular cross-sectioned channels for this study, the overall process for which is described below.

Layouts of the digitized network images were rendered in AutoCAD LT (AutoDesk, San Rafael, CA). The AutoCAD designs were printed at high resolution on Mylar film (CADArt, Poway, CA). The Mylar film was then used as a mask for ultra-violet (UV) light for patterning the desired thickness of positive resist (AZ P4620, Clariant, Somerville, NJ) spun on top of a silicon wafer. An adhesion promoter (Hexamethyldisilazane, HMDS, Sigma-Aldrich, St. Louis, MO) was used to enhance the strength of bonding of the photoresist on the silicon wafer. After developing for 3 min in the developer AZ 400K (Clariant, Charlotte, NC), the photoresist was overflown using a process known as photoresist reflow (Daly et al. 1990) by heating at 180°C for 2 min on a hotplate. The depth of the channels was measured using a Dektak profilometer (Veeco, Woodbury, NY) and found to be half of the width thus confirming the semicircular mold structures.

Sylgard 184 PDMS was prepared according to manufacturer's (Dow Corning, Midland, MI) instructions and cast over the photoresist mold to create complementary microchannels in PDMS. Through holes, defining the inlets and outlets, were punched using a beveled 25-gauge needle. The bonding surfaces of the PDMS and a pre-cleaned 1× 3 in. glass slide (Fisher Scientific, Pittsburgh, PA) were treated with oxygen plasma (150 mTorr, 50 W, 20 s) produced in the parallel plate plasma asher (March Inc., Concord, CA). A good seal between the PDMS and glass was achieved by heating the assembly at 75°C for 10 min on a hotplate yielding the semi-circular network. Tygon Microbore tubing with an outside diameter of 0.03 in. and inner diameter of 0.01 in. connected to 30 gauge stainless steel needle served as the connecting port to the syringe mounted on a programmable syringe pump. All the studies for this work were performed on networks with vessel diameters of 30 μm.

2.3 Experimental set-up

The inlet port (Fig. 3(a)) of the fabricated SMN was connected to a syringe mounted on a programmable syringe pump (PHD 2000, Harvard Apparatus, Holliston, MA) and placed on an inverted motorized stage (LEP Ltd, Hawthorne, NY) controlled by a computer. The networks were primed with ultrapure water and kept filled with water until the experiments. An epi-fluorescence microscope (TE 2000, Nikon Instruments Inc., Melville, NY) was used to capture images using a cooled CCD camera (SensiCam QE, Cooke Corporation, Romulus, MI) with a frame rate of 10 fps. The obtained images were post-processed using Image Pro Plus (Media Cybernetics, Inc., Bethesda, MD).

2.4 Perfusion in synthetic microvascular networks

Trypan blue (Sigma Aldrich, St. Louis, MO) was injected into the inlet port of the water-primed microvascular network at varying flow rates (0.05–5 μl/min). Images (×4 magnification) collected from adjacent microscope fields were digitized. These sequential images were then used to form a 6×6 montage of the microvascular network to determine the flow path in the network.

2.5 Particle transport in synthetic microvascular networks

Fluorescent particles with a diameter of 2 μm (Polysciences, Inc., Warrington, PA) were injected at varying flow rates (0.05–5 μl/min) at a concentration of 5×10^6 particles/ml into the inlet of the microvascular networks. Particle flow in the network and at the outlets was monitored over time. It was ensured that the flowing time was four to five times the volume of the entire network before data collection was started. For example, at a flow rate of 1 μl/min, images were collected approximately 10 min after injection using a ×10 magnification. Particle flux (number of particles per second) at junctions was measured by counting the number of particles entering the junction as well as the number of effluent particles over a 30 s time interval.

2.6 Anti-P-selectin and IgG coated microspheres

Fluorescent 2 μm microspheres (Polysciences Inc., Warrington, PA) at a concentration of 2×10^8 particles/ml were coated with anti-P-selectin antibody (BD Biosciences, San Jose, CA) or IgG (BD Biosciences, San Jose, CA). Microspheres were washed two times in 0.1 M

$NaHCO_3$ buffer pH 9.2. Following the wash steps, microspheres were incubated with Protein A (Zymed, Carlsbad, CA) at a concentration of 300 μg/ml and incubated at room temperature overnight to saturate the surface of the microsphere. The following day, a two times wash with solution containing 1% BSA in HBSS was performed. The microspheres were resuspended in 1% BSA in HBSS and incubated at room temperature for 20 min. Following incubation and subsequent two times wash with buffer, anti-P-selectin or IgG at a concentration of 100 μg/ml diluted in 1% BSA/HBSS was mixed with the microspheres. Protein A binds the Fc fragment of the antibody to allow proper orientation of the antibody and, as we have shown before, the concentration used ensures saturation of the surface of the microsphere with the antibody (Burch et al. 2002). The microspheres were held in this solution at 4° C until experimentation. Prior to experiments, microspheres were washed twice with 1% BSA and HBSS.

2.7 P-selectin coated synthetic microvascular networks

Microvascular network channels were injected with 10% SDS and 0.1 Triton X 100 at a flow rate of 1 μl/min for 5 min followed by a flow rate of 10 nl/min for 30 min. Following a wash, soluble human P-selectin (R&D Systems, Minneapolis, MN) at a concentration of 10 μg/ml was injected into the channel at a flow rate of 1 μl/min for 5 min followed by 50 nl/min for 10 min and allowed to incubate overnight in a humidified chamber at 4°C. Prior to the experiments, P-selectin coated networks were injected with 1% BSA solution at 10 nl/min and incubated for 30 min to minimize non-specific adhesion. Control SMNs (without P-selectin) were obtained in a similar way by flowing in 1% BSA in HBSS at a flow rate of 10 nl/min and allowed to incubate overnight at 4°C.

2.8 Synthetic microvascular network flow assay

Anti-P-selectin and IgG conjugated 2 μm fluorescent particles were injected at a concentration of 5×10^6 particles/ml into the inlet port of the fabricated microvascular networks at a flow rate of 1 μl/min for 10 min. The entire network was scanned for adherent particles. Any particle that did not move for 30 s was considered adherent.

2.9 P-selectin coated parallel plate flow chamber

Soluble human P-selectin at a concentration of 10 μg/ml was coated using a 5 mm flexiPERM gaskets (Greiner Bioone, Monroe, NC) mounted at the center of 35 mm tissue culture dishes. The inner region of the ring was outlined on the reverse side of the tissue culture dishes. Soluble P-selectin (50 μl) at a concentration of 10 μg/ml or HBSS (negative control) was placed inside the rings. The dishes were incubated at 4°C overnight in a humidified chamber, washed, and the entire dish flooded with 1% BSA in HBSS and incubated for 30 min prior to experiments.

2.10 Parallel plate flow chamber assay

A Glycotech flow chamber was assembled and placed on the microscope as described before (Prabhakarpandian et al. 2001). The fluid flow rate was adjusted to obtain the desired shear rate of 60 s^{-1}. The flow chamber was rinsed with buffer (HBSS, 1% BSA), and the flow of the anti-P-selectin conjugated 2 μm microspheres (1×10^6 particles/ml in HBSS, 1% BSA)

was initiated. The experiment was performed for 5–10 min and the number of adhering particles was counted. As before, any particle which did not move for 30 s, was considered adherent.

2.11 CFD model description

Experimental protocols dictated the set-up of steady fluid flow in the microfluidic networks followed by temporal studies of dye perfusion and particle transport/adhesion. Mathematical models to describe these phenomena are briefly discussed below.

2.12 Fluid flow models

Steady fluid flow is described by the conservation of fluid mass and momentum (Naviér–Stokes) equations (White 1991):

$$\frac{\partial u_i}{\partial x_i}=0 \quad \rho_c\frac{\partial u_i}{\partial t}+\rho_c\frac{\partial u_j u_i}{\partial x_j}=-\frac{\partial P}{\partial x_i}+\frac{\partial \tau_{ij}}{\partial x_j} \quad (1)$$

where u, ρ_c, P and g are the fluid velocity, density, pressure and gravity respectively. Fluid shear stress (τ_{ij}) is expressed in terms of the velocity profile using constitutive relations. For the purposes of this study, which used dilute aqueous buffers, an incompressible fluid following a Newtonian viscosity, model was assumed, i.e.,

$$\tau_{ij}=\mu_c\frac{\partial u_i}{\partial x_j} \quad (2)$$

Standard properties of water at room temperature (ρ_c = 1,000 kg/m^3, and μ_c = 0.001 kg·m^{-1}·s^{-1} were assumed. It must be noted that these relationships can be readily modified in future efforts to account for more realistic blood shear–viscosity relationships as needed. As boundary conditions, inlet flow rate was specified as set in the experiments and all outlets were set at atmospheric pressure.

2.13 Dye transport models

Unsteady dye perfusion was modeled by solving a convective-diffusive transport equation for a passive scalar:

$$\frac{\partial C_i}{\partial t}+\frac{\partial u_j C_i}{\partial x_j}=D_i\frac{\partial^2 C_i}{\partial x_j \partial x_j} \quad (3)$$

where C_i, and D_i are the dye concentration and diffusivity respectively. Dye diffusivity of 10^{-7} cm^2 s^{-1} was assumed. A conservative lower-bound value is used as we were primarily interested in evaluating the model prediction of the convection-driven axial filling pattern (filling order of the branches).

2.14 Particle transport models

Particle motion was tracked in a Lagrangian (following the particle) framework (Maxey and Riley 1983):

$$\frac{\partial v_i}{\partial t} = \frac{1}{\tau_v}(u_i - v_i) + g_i \quad (4)$$

where τ_v is the inertial relaxation time of the particle and g is the body force. The particle inertial relaxation time is calculated according to:

$$\tau_v = \frac{\rho_d}{\rho_c}\frac{d_p^2}{18v} \quad (5)$$

where ρ_d is the particle material density, ν is the fluid kinematic viscosity, and d_p is the diameter of the particle.

2.15 Particle adhesion models

Particle-wall interactions are triggered once a particle reaches within half the particle diameter of a wall. A stochastic adhesion model used to capture the inherently probabilistic nature of particle/cell adhesion process. In this model, the probability of particle adhesion is given by:

$$P = exp(-G/G_c) \quad (6)$$

where G is the local shear rate and G_c is the critical shear rate. The probability of adhesion resulting from a particle-wall interaction (or event) was computed and compared against a uniform random number. If the event led to adhesion, the particle location was arrested at the point of intersection. If the event did not result in adhesion, the particle was reflected at the wall by treating the boundary as a rigid body with infinite mass and inertia.

The critical shear rate is a function of particle size, as well as minimum and maximum bond length to represent the biochemical system. The functional form for the critical shear rate is taken to be:

$$G_c = K(sin\,\theta)^3 \quad \text{where} \quad \theta = cos^{-1}\left[1 - \frac{2(H-h)}{d_p}\right] \quad (7)$$

where K is a constant for a given receptor–ligand pair, H and h are the maximum and minimum bond length respectively and d_p is the particle diameter. This functional form of the critical shear rate (Hammer and Lauffenburger 1987) has been experimentally substantiated (Tees and Goetz 2003). Model parameters viz., K, H and h, were determined from *in vitro* flow chamber experiments (Fig. 2(a)) using 2 μm anti-P-selectin coated particles as described previously in particle adhesion assays sub-section.

2.16 Solution methodology

A general-purpose Computational Fluid Dynamics (CFD) code, CFD-ACE+ (Jiang and Przekwas 1994), based on the Finite Volume Method (FVM) was used to discretize and solve the governing equations. A computational mesh for the microvascular network was created by importing network layouts in DXF format into CFD-GEOM, the grid generation module of CFD-ACE+. The main purpose of the computational models is to facilitate

analysis of the experimental results by providing access and insight into experimentally inaccessible variables such as branch level shear and perfusion throughout the network. To this end, computational models of the network with rectangular cross-section were used as a first approximation. The generation of fully-circular or semi-circular channel geometry over a complex network is extremely challenging (especially at the junctions, where cylindrical surfaces intersect) and is beyond the intended scope of the current study. A three-dimensional hybrid mesh (Fig. 2(b)) comprising of hexahedral and prismatic elements, was created for subsequent simulation and analysis. Mesh refinement studies were performed to establish grid independence and the final computational domain consisted of approximately 160,000 nodes. For simulational prediction of particle flux, customized functions and subroutines were developed to monitor particle flux at an arbitrarily oriented plane.

3 Results and discussion

3.1 Perfusion in synthetic microvascular networks

Figure 3 shows the microscopic image of the fabricated SMN and a scanning electron micrograph showing the semi-circular cross-sectional geometry obtained in the channels. To our knowledge, this is the first microfluidic device comprising of semi-circular channels of microvascular networks. The network geometry used in the current study had one inlet and seven outlets.

Figure 4 shows the perfusion map of the networks over time following introduction of the Trypan Blue and the simulation predictions of dye perfusion for comparison. The level of perfusion in the network as predicted by the simulation is shown in a color coded scheme using an arbitrary concentration unit of the dye, with magenta representing complete perfusion and blue representing no perfusion. It can be seen that the predicted path of the dye as obtained from the simulations agrees very well with the actual path taken by Trypan Blue in the SMN. This confirms that flow resistances across the network are well predicted by the computational model. The results also suggest that perfusion in the networks may be spatially heterogeneous with the existence of under-perfused and/or stagnant regions, with implications for particle adhesion.

3.2 Particle transport in synthetic microvascular networks

Particle transport at a typical bifurcation in the SMN is shown in Fig. 5(a). The direction of particle transport at these junctions is indicated by arrows with Inlet (In) being the feeding vessel, and I and II denoting the subsequent fluid paths followed. Experimentally measured and predicted values of particle flux at several junctions were studied. The results showed good statistical agreement of modeled particle flux with the experimental data. The ratio of particle fluxes (termed particle split ratio) were defined with respect to the conditions in the feeding vessel (In) and the subsequent fluid paths denoted by I and II, respectively. We computed the particle split ratios at the junctions from the simulation results and compared them with experimental data (Fig. 5(b)). Division of particle flux into a major and minor arm was reproduced quantitatively in the model. While flow rates are difficult to measure concomitantly in the experiment, they are readily accessible from the simulation. Examining the relationship between flow split (defined the same way as particle split) and particle split

at this junction, we found that particle fluxes correlated reasonably well with the flow fluxes for this particle size and perfusion flow rate (Fig. 5(c)).

3.3 Particle adhesion in synthetic microvascular networks

Adhesion of Anti-P-selectin conjugated 2 μm particles to P-selectin coated SMN vessels was used to provide insight into the dynamics of particle deposition in the SMN. Figure 6(a) shows a snapshot of experimental observations where particle adhesion was found to be significantly localized near the bifurcations, as opposed to the linear branches. This finding (preferential particle adhesion in bifurcations) is in agreement with *in vivo* experimental observations (Yuan et al. 2005) and is a parameter that cannot be studied in conventional parallel plate flow chambers. Similar behavior was observed in the simulation model as well (Fig. 6(b)). Another observation was the predominance of particle adhesion in the central loop (denoted by label I), in comparison with other regions (denoted by label II and III).

To explain this observation and to develop a better understanding of the nature of the variation in adhesion processes in the SMN environment, we used the simulation models to generate a corresponding map of shear rate and perfusion across the entire network (Fig. 7). For these maps, the shear and velocities were obtained from the CFD simulations by volumetrically averaging over a particular junction or branch. Particle adhesion was found to be minimal in high shear regions (as exemplified by region II). Moderate shear regions (region I) showed more adhesion compared with very low shear regions (region III). Here we use the terms low, moderate and high shear to represent values of <30, 30–120 and >120 s^{-1}, respectively.

It must be noted that in simple, idealized network constructions (linear forward flow, constant cross-section) perfusion and shear rate are directly related. However, in *in-vivo* situations the relationship is more complicated. For instance, circulating flow loops provide shear but have no net perfusion while during cross-sectional changes perfusion rate remains the same while shear changes. Particle transport into the channel is then related to the volumetric perfusion rate, while adhesion is primarily dictated by wall or surface shear. Overall particle adhesion is maximized in situations where perfusion is maximized while minimizing shear. Such effects, while difficult to highlight individually, are intrinsically represented in the computational and *in-vitro* methods described here.

3.4 Comparison with parallel plate flow chamber

As an illustration of the range of information obtained from even a single set of experiments and associated fluidic analysis in the SMN, a shear-adhesion diagram over the entire network was prepared. The shear-adhesion diagram refers to a plot of the number of adhered particles, as a function of shear rate, typically normalized by a particle number invariant across the experiments. This is generally the number of particles in solution or that adhered to the substrate at zero shear (incubation). An equivalent procedure is not possible in SMN experiments, as particle perfusion rates vary non-uniformly in the various arms and must be individually corrected for, in order to yield the true dependence on shear. Using a global number based on input particle concentrations is likely to be misleading. While the

experimentally measured number of particles entering a particular vessel segment is an obvious choice, it is difficult to measure.

However, given the good agreement between experimental and simulated particle fluxes (as shown in Fig. 6(b) and (c)), the CFD model data provides an alternative avenue for correcting particle adhesion data with particle perfusion to each individual branch. In our procedure, the simulation results were used to determine the number of particles colliding with the wall in each branch. The term “collision” here refers to the number of particles that contact the wall (i.e., particle trajectories that are computed to intersect with the wall). Using this measure, the fraction of adhered particles was calculated by taking the experimentally observed number of firmly adhered particles and dividing by the model-derived number of particle–wall collisions as calculated for the individual vessel segment, i.e.,

$$\%\text{Adhesion} = \frac{\text{Number of particles adhered (experiments)}}{\text{Number of particle}-\text{wall collisions (simulations)}} \quad (8)$$

In effect, this metric is- a direct measure of the efficiency of the adhesion process. The resulting shear-adhesion diagram shown in Fig. 8 displays the well-known monotonic decrease in fraction of adhered particles with shear rate (or stress), as seen from classical parallel plate flow chamber experiments (as shown in Fig. 2(a)). Other normalizing measures such as the total number (or flux) of particles in each individual segment (also obtained from the model) were seen to yield qualitatively the same results as shown here.

However, it is important to note that, while in parallel plate flow chambers a number of experiments are necessary to establish this correlation between particle adhesion and shear rate, in the SMNs this correlation can be established in one experiment by measuring particle adhesion in various sections of the network. Additionally, in parallel plate flow chambers, multiple experiments necessitate a large amount of consumables (reagents and particles). Compared to a typical flow chamber experiment, the SMN offers significant savings in both time and reagents. Table 1 summarizes expected typical savings in reagents using SMN flow chambers.

4 Conclusions

We have developed a methodology for image-derived, anatomically realistic synthetic microvascular networks (SMN) that could be fabricated and used to generate novel insights into the adhesion process with understanding being provided by the accompanying CFD analysis. These studies highlight the spatial heterogeneity of the microvascular networks and the need to sufficiently represent and account for the complex morphology of the microvasculature. Dye perfusion studies indicated the presence of well perfused as well as stagnant regions in a given network. Particle adhesion was also found to be non-uniform and predominant at microvessel junctions. These findings could not have been readily identified with existing flow chambers such as the parallel plate flow chamber or CFD models alone.

Our findings clearly point to the value of using the *in vitro* microvascular flow chamber developed in this study to gain better insights into and a more accurate quantitative analysis

of particle and cell adhesion in the microvasculature. Using these networks, a single experiment was used to generate an entire shear-adhesion diagram and thus can potentially replace a plethora of parallel plate flow chamber experiments in addition to offering savings of over two orders of magnitude in reagents. We are currently extending the techniques developed in this study to microvascular networks from other tissue including mesentery and brain. A more fundamental study on the relationship between microvessel junction topologies and particle adhesion is underway. Finally, we are developing protocols for successful endothelial cell culture in these microvascular networks for studying particle adhesion and uptake. Other potential applications of the SMN could include shear related studies of cell adhesion, cell migration, drug delivery vehicle screening, vascular-targeted therapies, and basic research on microcirculation related phenomena in both normal and diseased tissues.

Acknowledgements

The authors would also like to thank Dr. Bin Wang for help during the dye perfusion studies. We gratefully acknowledge financial support from NIH (2R44HL076034-02).

References

Anderson JR, Chiu DT, Jackman RJ, Cherniavskaya O, McDonald JC, Wu H, Whitesides SH, Whitesides GM. Anal. Chem. 2000; 72:3158–3164. [PubMed: 10939381]

Bendas G, Krause A, Bakowsky U, Vogel JJ, Rothe U. Int. J. Pharm. 1999; 181:79–93. [PubMed: 10370205]

Blackwell JE, Dagia NM, Dickerson JB, Berg EL, Goetz DJ. Ann. Biomed. Eng. 2001; 29:523–33. [PubMed: 11459346]

Bloemen PGM, Henricks PAJ, Van Bloois L, Van den Tweel MC, Bloem AC, Nijkamp FP, Crommelin DJA, Storm G. FEBS Lett. 1995; 357:140–144. [PubMed: 7805880]

Brown DC, Larson RS. BMC Immunol. 2001; 2:9. [PubMed: 11580861]

Burch EE, Shinde Patil VR, Camphausen RT, Kiani MF, Goetz DJ. Blood. 2002; 100:531–538. [PubMed: 12091345]

Carlos TM, Harlan JM. Blood. 1994; 84:2068–2101. [PubMed: 7522621]

Cokelet GR, Soave R, Pugh G, Rathbun L. Microvasc. Res. 1993; 46:394–400. [PubMed: 8121322]

Cotran RS, Mayadas-Norton T. Pathol. Biol. (Paris). 1998; 46:164–70. [PubMed: 9769911]

Cozens-Roberts C, Quinn JA, Lauffenberger DA. Biophys. J. 1990; 58:107–25. [PubMed: 2166596]

Crutchfield KL, Shinde Patil VR, Campbell CJ, Parkos CA, Allport JR, Goetz DJ. J. Leukoc. Biol. 2000; 67:196–205. [PubMed: 10670580]

Daly D, Stevens RF, Hutley MC, Davies N. Meas. Sci. Technol. 1990; 1:759–766.

Dickerson JB, Blackwell JE, Ou JJ, Shinde Patil VR, Goetz DJ. Biotechnol. Bioeng. 2001; 73:500–509. [PubMed: 11344455]

El-Ali J, Sorger PK, Jensen KF. Nature. 2006; 442:403–11. [PubMed: 16871208]

El-Sayed M, Kiani MF, Naimark MD, Hikal AH, Ghandehari H. Pharm. Res. 2001; 18:23–8. [PubMed: 11336349]

Frame MDS, Sarelius IH. Microcirculation. 1995; 2:377–385. [PubMed: 8714819]

Gaehtgens P. Int. J. Microcirc. Clin. Exp. 1992; 11:123–132. [PubMed: 1612826]

Gerritsen ME. Biochem. Pharmacol. 1987; 36:2701–2711. [PubMed: 2820420]

Goetz DJ, el-Sabban ME, Pauli BU, Hammer DA. Biophys. J. 1994; 66:2202–2209. [PubMed: 7521229]

Goetz DJ, Greif DM, Ding H, Camphausen RT, Howes S, Comess KM, Snapp KR, Kansas GS, Luscinskas FW, Cell Biol J. 1997; 137:509–19.

Goldsmith HL, Turitto VT. Thromb. Haemost. 1986; 55:415–35. [PubMed: 3750272]

Hajitou A, Pasqualini R, Arap W. Trends Cardiovasc. Med. 2006; 16:80–88. [PubMed: 16546688]

Hammer DA, Lauffenburger DA. Biophys. J. 1987; 52:475–87. [PubMed: 2820521]

Jiang Y, Przekwas AJ. 1994 AIAA-94-0303.

Kiani MF, Yuan Y, Chen X, Smith L, Gaber MW, Goetz DJ. Pharm. Res. 2002; 19:1317–1322. [PubMed: 12403068]

Kluger MS. Adv. Dermatol. 2004; 20:163–201. [PubMed: 15544200]

Lu H, Koo LY, Wang WM, Lauffenburger DA, Griffith LG, Jensen KF. Anal. Chem. 2004; 76:5257–64. [PubMed: 15362881]

Luscinskas FW, Kansas GS, Ding H, Pizcueta P, Schleiffenbaum B, Tedder TF, Gimbrone MA Jr. J. Cell Biol. 1994; 125:1417–1427. [PubMed: 7515891]

Maxey MR, Riley JJ. Phys. Fluids. 1983; 26:883–889.

Moghimi SM, Hunter AC, Murray JC. FASEB J. 2005; 19:311–330. [PubMed: 15746175]

Molla M, Panes J. World J. Gastroenterol. 2007; 13:3043–3046. [PubMed: 17589918]

Muller MM, Griesmacher A. Clin. Chem. Lab. Med. 2000; 38:77–85. [PubMed: 10834393]

Nahmias Y, Berthiaume F, Yarmush ML. Adv. Biochem. Eng. Biotechnol. 2007; 103:309–29. [PubMed: 17195468]

Nguyen V, Gaber MW, Sontag MR, Kiani MF. Radiat. Res. 2000; 154:531–536. [PubMed: 11025649]

Pasyk KA, Jakobczak BA. Eur J Dermatol. 2004; 14:209–13. [PubMed: 15319151]

Patel KD. J. Immunol. 1999; 162:6209–16. [PubMed: 10229866]

Patil VR, Campbell CJ, Yuan YH, Slack SM, Goetz DJ. Biophys. J. 2001; 80:1733–1743. [PubMed: 11259287]

Patillo CB, Sari-Sarraf F, Nallamothu R, Moore BM, Wood GC, Kiani MF. Pharm. Res. 2005; 22:1117–1120. [PubMed: 16028012]

Prabhakarpandian B, Goetz DJ, Swerlick RA, Chen X, Kiani MF. Microcirculation. 2001; 8:355–64. [PubMed: 11687947]

Rao RM, Yang L, Garcia-Cardena G, Luscinskas FW. Circ. Res. 2007; 101:234–47. [PubMed: 17673684]

Roth NM, Kiani MF. Ann. Biomed. Eng. 1999; 27:42–47. [PubMed: 9916759]

Roth NM, Sontag MR, Kiani MF. Radiat. Res. 1999; 151:270–277. [PubMed: 10073664]

Sakhalkar HS, Dalal MK, Salem AK, Ansari R, Fu J, Kiani MF, Kurjiaka DT, Hanes J, Shakesheff KM, Goetz DF. Proc. Natl. Acad. Sci. 2003; 100:15895–15900. [PubMed: 14668435]

Scott RC, Wang B, Nallamothu R, Pattillo CB, Perez-Liz G, Issekutz AC, Del Valle L, Wood GC, Kiani MF. Biotechnol. Bioeng. 2007; 96:795–802. [PubMed: 17051598]

Spragg DD, Alford DR, Greferath R, Larsen CE, Lee KD, Gurtner GC, Cybulsky MI, Tess DFJ, Goetz DJ. News Physiol. Sci. 2003; 18:186–190. [PubMed: 14500796]

Springer TA. Cell. 1994; 76:301–314. [PubMed: 7507411]

Tees DFJ, Goetz DJ. News Physiol. Sci. 2003; 18:186–190. [PubMed: 14500796]

White, FM. Viscous Fluid Flow. McGraw-Hill; New York, NY: 1991.

Yuan H, Goetz DJ, Gaber MW, Issekutz AC, Merchant TE, Kiani MF. Radiat. Res. 2005; 163:544–551. [PubMed: 15850416]

Zou X, Shinde Patil VR, Dagia NM, Smith LA, Wargo MJ, Interliggi KA, Lloyd CM, Tess DF, Walcheck B, Lawrence MB, Goetz DJ. Am. J. Physiol. Cell Physiol. 2005; 289:C415–24. [PubMed: 15814589]

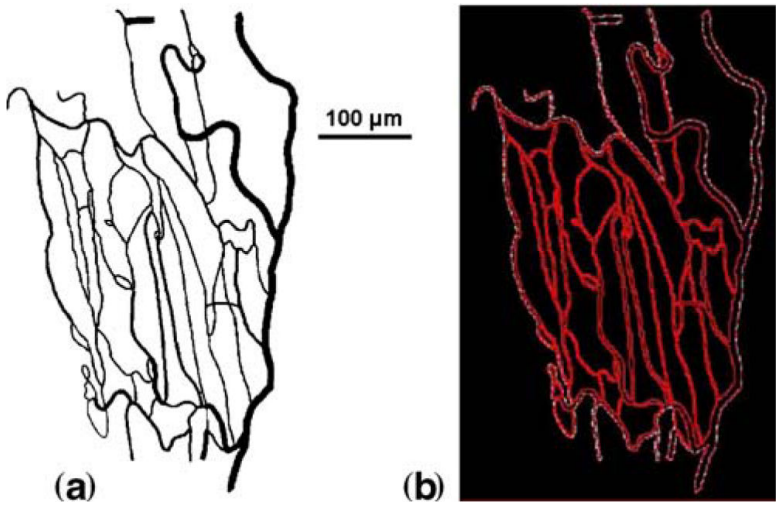

Fig. 1.

(**a**) The vessels in the network were digitized using the software Arc-Info. (**b**) The digitized image was vectorized to obtain the image containing the connectivity information on the network. Flow directions observed *in vivo* defined the inlet/outlet ports of the network

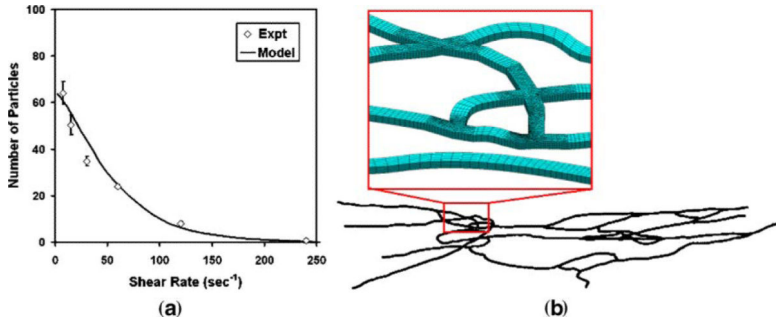

Fig. 2.

(**a**) The computational model was calibrated with *in vitro* flow chamber experimental data using P-selectin on the surface and anti-P selectin antibody coated 2 μm particles. The fitted parameter values were found to be as follows: $K=4\times10^3$ s^{-1}; H=120 nm, h=10 nm. (**b**) A typical computational mesh of the microvascular networks (~160,000 computational cells)

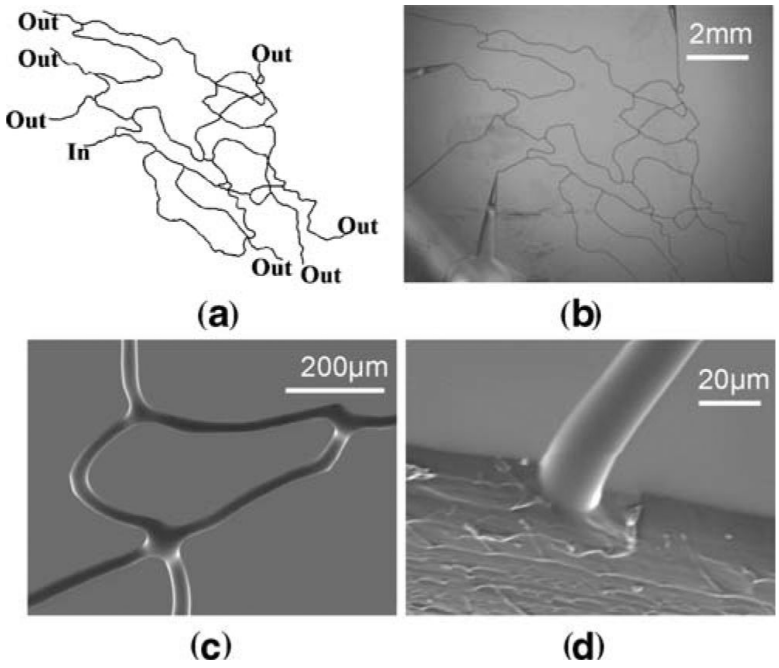

Fig. 3.

(**a**) Schematic showing the inlet and outlet ports of the network. (**b**) Microvascular network created on PDMS. (**c**) Magnified view of a junction in the network. (**d**) Scanning electron micrograph of vessel showing semi-circular channels

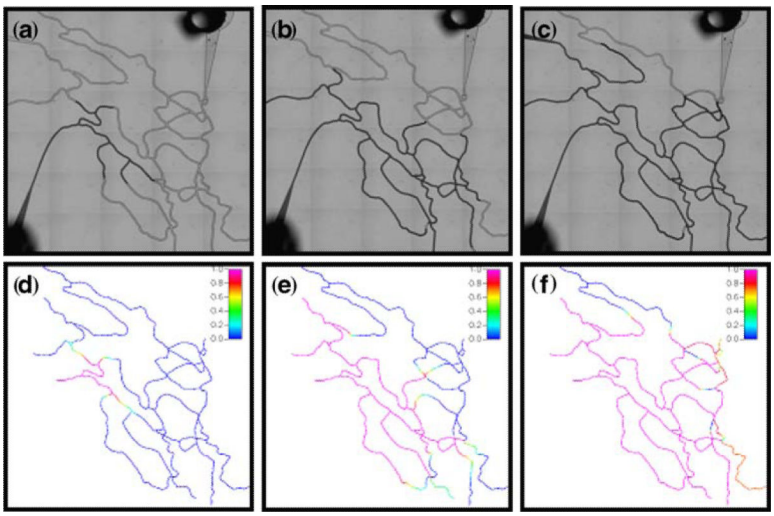

Fig. 4.

Transient perfusion studies comparing experimental and simulation results in SMN. (**a–c**) Experiments and (**d–f**) simulation. The scale for simulation is an arbitrary unit with *blue* (no perfusion; 0) and *magenta* (complete perfusion; 1). The flow rate was 0.05 μl/min and 35 frames were taken with a delay of 1 min and 25 s between each frame for a total of 50 min. Experimental and simulation results show very good comparison with each other

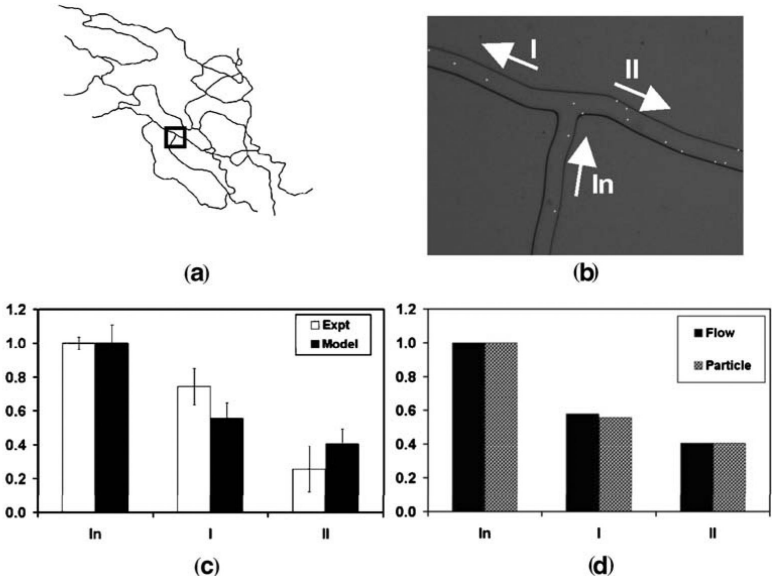

Fig. 5.

(**a**) Bifurcation location in the network. (**b**) Particle flux at the bifurcation with inlet (*In*) being the feeding vessel and *I*, and *II* denoting the subsequent fluid paths followed. (**c**) Comparison of experimentally measured and model predicted particle split ratio at the bifurcation at In, I and II with the standard deviation. Each experiment was repeated three times. The *error bars* in the computational results appears due to the fact that particle transport and adhesion simulations were run in an unsteady manner. Time data was averaged over a 30 s interval to calculate the particle fluxes (number per second). (**d**) Flow and particle split correlation at the bifurcation (from simulation)

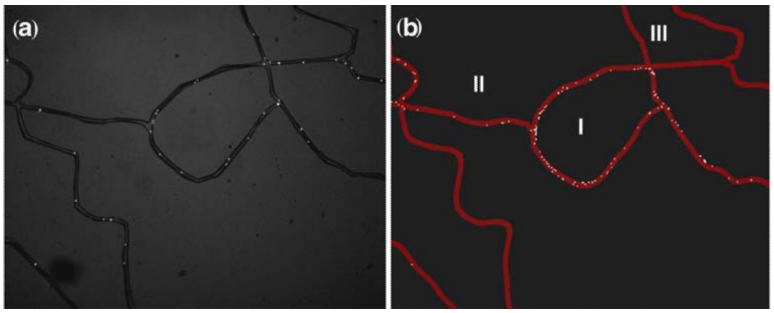

Fig. 6.

Particle adhesion in a sample section of the microvascular network. (**a**) Experiment. (**b**) Simulation. Particle adhesion was measured 10 min after injection of anti-P-selectin or IgG coating particles

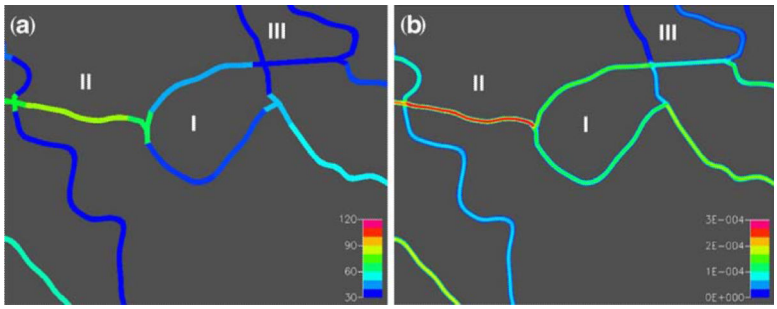

Fig. 7.

(**a**) Shear rate variation in the corresponding microvascular network section (legend values of s^{-1}). (**b**) Perfusion velocity variation (legend values in meters per second). *I* Moderate perfusion and shear, *II* high perfusion and shear, *III* low perfusion and shear. Here we use the terms low, moderate and high shear to represent values of <30, 30–120 and >120 s^{-1} respectively

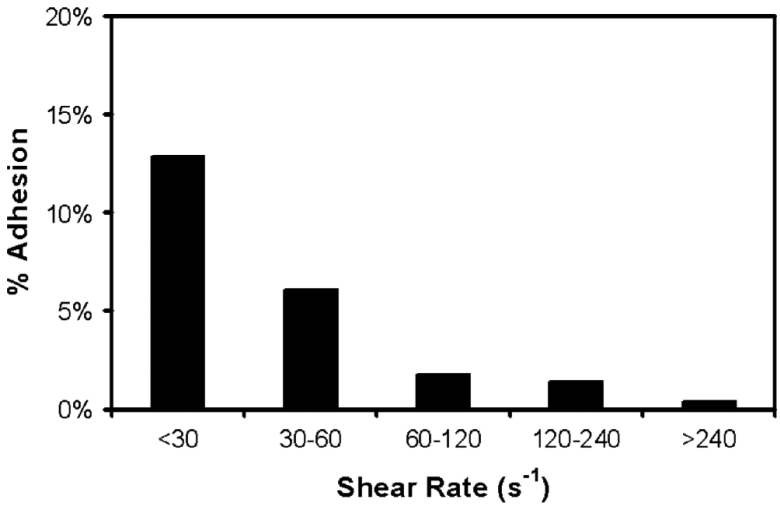

Fig. 8.

Shear-adhesion plot obtained from the microvascular network. The entire network was scanned to measure the number of particles. The corresponding shear rate at the location was obtained from the simulation results

Table 1

Comparison of synthetic microvascular network with *in vitro* flow chamber (values for parallel plate flow chamber assays are for a typical assay with a shear rate of 60 s^{-1}, particle concentration of 1E6 particles/ml and duration of 3 min for adhesion

Adhesion platform	Reagent volume (μ1)	Number of particles per experiment	Dead volume in tubing (μ1)
Typical flow chamber	50–2,000	5E+05	32.0
Microvascular network	1	5E+02	3.0
% Savings	>98	>99	>90

Inlet tubing size is taken to be 0.8 mm ID. Values for microfluidic microvasculature chip are for same shear rate, particle concentration of 5E6 particles/ml, duration of 10 min for adhesion and tubing size of 0.25 mm ID)